

CLOCK SKEW CALIBRATION FOR UWB RANGING

Yiyin Wang, Zijian Tang, and Geert Leus

Delft University of Technology, Fac. EEMCS, Mekelweg 4, 2628CD Delft, The Netherlands

ABSTRACT

In this paper, we propose a clock skew calibration method for ranging applications using an ultra-wideband (UWB) signal. The clock skew is one of the main error sources in time-of-arrival (TOA) based UWB ranging, since a long ranging signal is required to obtain a sufficiently high signal-to-noise ratio (SNR). Therefore, the clock skew calibration is essential for accurate TOA ranging. We propose to estimate the clock skew in the frequency domain to take full advantage of the periodic property of the ranging signal, which allows the proposed method to reach super-resolution. Simulation results corroborate the efficiency of the proposed method.

1. INTRODUCTION

Ultra-wideband (UWB) impulse radio (IR) is a promising technology for high resolution ranging [1, 2]. Using UWB IR, the multipath channel components can be resolved, and if we can detect the first arriving multipath component, we can estimate the time-of-arrival (TOA) with high resolution, which facilitates accurate ranging. In order to obtain high accuracy TOA estimation, a long ranging signal composed of many frames is normally employed to enhance the received signal-to-noise ratio (SNR) [1]. However, due to many error sources, such as temperature and low-cost crystals, there is a clock discrepancy between the transmitter and the receiver clock. We refer to this clock discrepancy as a relative clock skew, which describes the frequency difference between the two clocks. As a result, the same ranging signal can be viewed differently due to this clock skew. Therefore, it is essential to carry out a clock skew calibration in order to achieve accurate TOA estimation [3, 4, 5]. Some time-domain approaches have been proposed in [4, 5] to solve this problem. However, they have to perform a complex search through trellis-based paths.

In this paper, we investigate a frequency-domain approach to estimate the clock skew. We make use of the periodic property of the ranging signal, which manifests itself as local peaks following a well-defined pattern in the frequency domain. The clock skew information is embedded in the distance between these local peaks. Instead of estimating the average distance between local maxima, which is quite challenging due to the multipath channel, we assume the knowledge of the frequency pattern and try different numbers of zeros padded to the end of the ranging signal, and search for the most appropriate zero-padded signal, which can collect the maximum energy from the known frequency pattern. The most appropriate length of the zero-padded signal should be an integer multiple of the frame period. Hence, we can derive the clock skew based on the above information. We start with the system model in Section 2. The frequency domain analysis follows in Section 3. The frequency domain method for the clock skew estimation is proposed in Section 4. Simulation results are shown in Section 5.

2. SYSTEM MODEL

We design a ranging signal composed of several frames. Each frame is of period T_f and hosts one pulse. The transmitted signal can then be written as $s(t) = \sum_{i=0}^{N-1} p(t - iT_f)$, where $p(t)$ is the transmitted pulse shape, and N is the total number of frames. After propagation through a multipath channel $h(t)$, the received signal is filtered by a front-end filter $g(t)$. Consequently, the received signal in the noiseless case can be modeled as

$$\begin{aligned} x(t) &= g(t) * h(t) * s(t) \\ &= \sum_{l=0}^{L-1} \sum_{i=0}^{N-1} \alpha_l \phi(t - iT_f - \tau_l), \end{aligned} \quad (1)$$

where $*$ denotes convolution; $h(t) = \sum_{l=0}^{L-1} \alpha_l \delta(t - \tau_l)$ is the multipath channel impulse response with α_l and τ_l representing the amplitude and arrival time of the l th path, respectively, and $\phi(t) = g(t) * p(t)$. Without loss of generality, we let $0 \leq \tau_0 < \tau_1 < \dots < \tau_{L-1}$, and thus the time-of-arrival (TOA) of the ranging signal is equal to τ_0 . We assume that T_f is long enough, i.e., $T_f > \tau_{L-1} - \tau_0 + T_\phi$, where T_ϕ is the length of $\phi(t)$, such that there is no inter-frame interference (IFI). Furthermore, we assume that the whole received ranging signal is subsumed in an observation window, which starts at $t = 0$, and is of length T_o . Hence, $T_o > NT_f + \tau_0$. In addition, this observation window contains no other signals.

If the frame period T_f is perfectly known, then the TOA can be accurately estimated by adopting super-resolution methods, such as MUSIC [6]. However, due to many error sources, such as temperature and low-cost crystals, there is a clock discrepancy between the transmitter and the receiver. We refer to this clock discrepancy as the relative clock skew, which remains constant during the TOA estimation. If we consider sampling the received signal, the receiver's sampling period is a scaling of the transmitter's sampling period. It is more convenient to assume that the receiver clock does not change, the received signal is a scaling of the received one without the relative clock skew. Hence, we use $\tilde{x}(t)$ to denote the received signal when there is a relative clock skew between the transmitter and the receiver, which is a scaled version of $x(t)$ defined as

$$\tilde{x}(t) = x\left(\frac{t}{1 + \Delta}\right), \quad (2)$$

where $1 + \Delta$ defines the relative clock skew and Δ denotes the relative clock skew difference to be estimated. The typical range of Δ is from -80 ppm to 80 ppm according to the IEEE 802.15.4a standard [1]. Although $|\Delta| \ll 1$, the accumulated clock drift over the whole ranging signal¹ due to Δ can lead to serious problems in TOA estimation [4, 5]. In order to estimate the TOA accurately, the knowledge of Δ is indispensable.

¹The length of the ranging signal could be several milliseconds according to [1].

3. FREQUENCY-DOMAIN ANALYSIS

Note that the ranging signal periodicity remains even in the presence of a relative clock skew. For estimation, it will be instrumental that we first investigate the relationship among the continuous Fourier transform (CFT), the discrete-time Fourier transform (DTFT) and the discrete Fourier transform (DFT) of $x(t)$. Let us define the CFT of $\phi(t)$ and $x(t)$ as $\Phi(f)$ and $X(f)$, respectively. Obviously,

$$X(f) = \int_{-\infty}^{+\infty} x(t)e^{-j2\pi ft} dt = \int_0^{NT_f} x(t)e^{-j2\pi ft} dt. \quad (3)$$

Note that $X(f)$ is independent of the observation window length T_o , but related to the length of the ranging signal NT_f . Using $\text{rect}(t)$ to define a rectangular window that equals 1 for $-1/2 \leq t \leq 1/2$ and 0 otherwise, and realizing that

$$\begin{aligned} & \mathcal{F} \left(\text{rect} \left(\frac{t}{NT_f} - \frac{1}{2} \right) \sum_{i=-\infty}^{+\infty} \delta(t - iT_f) \right) \\ &= N e^{-j\pi NT_f f} \sum_{i=-\infty}^{+\infty} e^{j\pi Ni} \text{sinc} \left(NT_f \left(f - \frac{i}{T_f} \right) \right), \quad (4) \end{aligned}$$

we arrive at

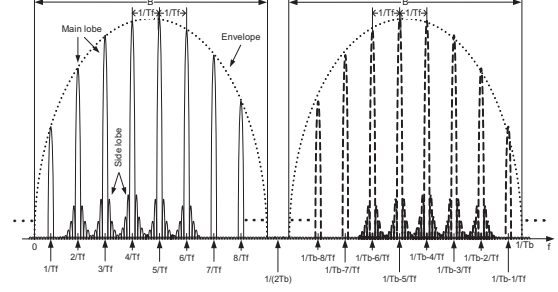
$$\begin{aligned} X(f) &= N \Phi(f) e^{-j\pi NT_f f} \sum_{l=0}^{L-1} \alpha_l e^{-j2\pi \tau_l f} \\ &\quad \times \sum_{i=-\infty}^{+\infty} e^{j\pi Ni} \text{sinc} \left(NT_f \left(f - \frac{i}{T_f} \right) \right), \quad (5) \end{aligned}$$

which is a sum of an infinite number of sinc pulses, whose amplitudes are modulated by $N \Phi(f) e^{-j\pi NT_f f} \sum_{l=0}^{L-1} \alpha_l e^{-j2\pi \tau_l f}$. The function $|X(f)|$ in the range of $[0, 1/(2T_b)]$ is illustrated in the left half of Fig. 1, where T_b is a value satisfying $1/T_b \geq 2B$, with B denoting the single-sided bandwidth of $\phi(t)$, which does not have any DC components (obviously, the bandwidth of $x(t)$ is determined by $\phi(t)$). The main lobe (or side lobe) of the sinc pulse has a width of $2/(NT_f)$ (or $1/(NT_f)$), which thus depends on the length of the ranging signal. The distance between two adjacent main-lobe peaks is $1/T_f$, and there are in total $\lfloor T_f/(2T_b) \rfloor$ main lobes in the frequency range $[0, 1/(2T_b)]$. At the main-lobe peak of each sinc pulse ($f = i/T_f, i = -\infty, \dots, +\infty$), the influence of the side lobes from the other sinc pulses vanishes. However, the side-lobe effect remains at other frequencies, which may result in changing the main-lobe shape. But when N is large enough, the side-lobe effect can be ignored. Moreover, $X(f) = 0$, when $f = i'/(NT_f), i' = -\infty, \dots, +\infty$ and $f \neq i/T_f, i = -\infty, \dots, +\infty$. Here, we underline that it is the total length of the ranging signal NT_f , not the length of the observation window T_o , that decides the main-lobe width of the sinc pulse. Therefore, the spectrum leakage due to the limited length of the ranging signal is determined by NT_f , and T_o does not play any role in $X(f)$.

Now let us sample $x(t)$ at rate $1/T_b$. Then the DTFT $\bar{X}(f)$ of the sampled $x(t)$ can be obtained as

$$\bar{X}(f) = \sum_{n=-\infty}^{+\infty} x(nT_b) e^{-j2\pi n T_b f} = \frac{1}{T_b} \sum_{i=-\infty}^{+\infty} X \left(f - \frac{i}{T_b} \right), \quad (6)$$

according to the Poisson summation formula. Due to the sampling effect, $\bar{X}(f)$ is a periodical extension of $X(f)$ with period $1/T_b$. With $1/T_b \geq 2B$, spectrum aliasing can be ignored. Fig.1 shows such an example. Recall that the positions of the main-lobe peaks



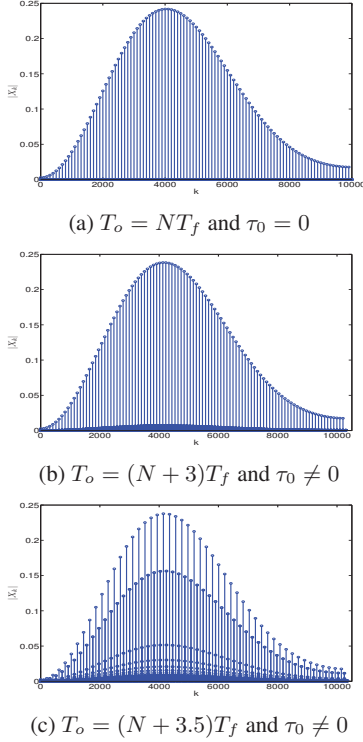


Fig. 2. Examples of $|X_k|$, different T_o , a single path channel

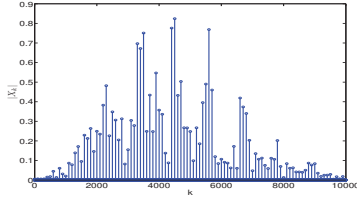


Fig. 3. an example of $|X_k|$, $T_o = NT_f$ and $\tau_0 = 0$, a multipath channel

with an equi-distant pattern, i.e., these main-lobe peaks are separated in X_k with $K - 1$ non-zero samples. Fig. 2(c) indicates the situation, where the observation window $T_o = KT_f$ with $K = N + 3.5$ being a non-integer, and $\tau_0 \neq 0$. As a consequence, the main-lobe peaks in $\tilde{X}(f)$ are missed, although we can still obtain some samples for the main lobes. Accordingly, the energy contained in these points will be lower than that in Fig. 2(a) and Fig. 2(b). In Fig. 3, we use a multipath channel, which is composed of 10 multipath components. The amplitudes of the multipath components follow a zero-mean Gaussian distribution, and the delays are uniformly distributed in the range of $[0, T_f - T_p]$. As can be seen, the envelope of $|X_k|$ has an irregular shape, which is determined by both $\Phi(f)$ and the multipath channel. Since we employ $T_o = NT_f$ and $\tau_0 = 0$, $|X_k|$ still follows the same frequency pattern concerning the positions of the main-lobe peaks and zeros. Comparing Fig. 2(a) with Fig. 3, we observe that the multipath channel dramatically changes the amplitude of the main-lobe peaks of X_k , which now has sharp variations.

As we have mentioned before, due to the relative clock skew between the transmitter and the receiver clock, the received signal

$\tilde{x}(t)$ is a kind of scaled version of $x(t)$ given by (2). Making use of the convolution and the scaling property of the Fourier transform, the CFT $\tilde{X}(f)$ of $\tilde{x}(t)$ is given by

$$\tilde{X}(f) = N(1 + \Delta)\Phi((1 + \Delta)f) e^{-j\pi NT_f(1 + \Delta)f} \sum_{l=0}^{L-1} \alpha_l e^{-j2\pi\tau_l(1 + \Delta)f} \times \sum_{i=-\infty}^{+\infty} e^{j\pi Ni} \text{sinc}\left(NT_f\left((1 + \Delta)f - \frac{i}{T_f}\right)\right). \quad (9)$$

$\tilde{X}(f)$ has a similar frequency pattern as $X(f)$. However, we remark that the main-lobe width of the sinc pulse is now $2/(NT_f(1 + \Delta))$. The distance between two adjacent main-lobe peaks is $1/(T_f(1 + \Delta))$. Then, $\tilde{X}(f)$ can be similarly depicted as in Fig. 1, except that we need to replace T_f with $T_f(1 + \Delta)$ in the figure. Accordingly, we consider an observation window of length

$$\tilde{T}_o = \tilde{K}T_f(1 + \Delta), \quad (10)$$

satisfying that $\tilde{T}_o > NT_f(1 + \Delta) + \tau_0$. We still sample $\tilde{x}(t)$ at rate $1/T_b$, assuming that the Nyquist sampling requirement is still met. We obtain a batch of samples $\tilde{x}_n = \tilde{x}(nT_b)$, where $n = 0, 1, \dots, \lfloor \tilde{T}_o/T_b \rfloor - 1$. The DFT \tilde{X}_k of \tilde{x}_n is calculated as

$$\tilde{X}_k \approx \frac{1}{T_b} \left(\tilde{X}\left(\frac{k}{\tilde{T}_o}\right) + \tilde{X}\left(\frac{k}{\tilde{T}_o} - \frac{1}{T_b}\right) \right), k=0, \dots, \left\lfloor \frac{\tilde{T}_o}{T_b} \right\rfloor - 1, \quad (11)$$

Similar to the previous case without clock skew, we are able to attain the following two properties for $\tilde{X}(f)$ and \tilde{X}_k .

Property 1 The frequency distance between two adjacent local peaks of $\tilde{X}(f)$ is $1/(T_f(1 + \Delta))$.

Property 2 If \tilde{K} is an integer, the local maxima of \tilde{X}_k will also coincide with the main-lobe peaks of $\tilde{X}(f)$.

4. RELATIVE SKEW DIFFERENCE ESTIMATION

Intuitively, the estimation of Δ can be achieved by making use of Property 1 and estimating the average distance between every two adjacent local maxima of $\tilde{X}(f)$. However, it is not trivial to achieve this due to the following reasons: i) we only have \tilde{X}_k as an approximation of $\tilde{X}(f)$; and ii) localizing the local maxima of \tilde{X}_k can be an extremely challenging problem due to the multipath channel, as the amplitudes of \tilde{X}_k become much less predictable as shown in Fig. 3. The situation gets even worse if the received signal is also subject to noise.

A less straightforward method is to resort to Property 2: assuming the knowledge of the integer multitude \tilde{K} , we try to collect the maximum energy from the known frequency pattern according to \tilde{K} by padding different numbers of zeros to the end of the ranging signal. To be more specific, making use of $0 \leq \tau_0 < N_\tau T_f^2$, and Δ_{\max} ($\Delta \in [-\Delta_{\max}, \Delta_{\max}]$), we can first construct a fixed observation window \tilde{T}_{of} as $\tilde{T}_{of} = (N + N_\tau)T_f(1 + \Delta_{\max})$, to limit the pure noise samples. As a result, we obtain $\tilde{x}_n, n = 0, 1, \dots, L_r - 1$, and $L_r = \lfloor \tilde{T}_{of}/T_b \rfloor$. We can then try L zeros padded at the end of \tilde{x}_n , where $L \in \mathcal{R}_L(\tilde{K})$, and $\mathcal{R}_L(\tilde{K}) = \{L_o, L_o + 1, \dots, L_o + 2L_\Delta\}$. Moreover, $L_o = \lfloor \tilde{K}T_f(1 - \Delta_{\max})/T_b \rfloor - L_r$, and $L_\Delta =$

² N_τ can be obtained by a simple energy detection and $N_\tau \ll N$

$\lceil \tilde{K}T_f \Delta_{\max}/T_b \rceil$, which is the maximum number of samples resulting from the maximum accumulated drift over the whole observation window. As $L_o \geq 0$, then $\tilde{K} \geq \tilde{K}_{\min}$, where $\tilde{K}_{\min} = \lceil (N + N_\tau)(1 + \Delta_{\max})/(1 - \Delta_{\max}) \rceil$. Therefore, \tilde{K} could be any integer no less than \tilde{K}_{\min} . Then, we examine the energy sum collected at the points \tilde{X}_k for $k = 0, \tilde{K}, \dots, (L_{f/2} - 1)\tilde{K}$, where $L_{f/2} = \lceil T_f(1 + \Delta_{\max})/(2T_b) \rceil$. Since $\tilde{x}(t)$ is a real signal, we only use $L_{f/2}$ samples of \tilde{X}_k to reduce the computational complexity. Suppose with \hat{L} zero padded, the resulting energy sum is maximized. It then follows that $\tilde{T}_o = (L_r + \hat{L})T_b$. With the knowledge of \tilde{T}_o as well as \tilde{K} , Δ can be derived. The above operations can be mathematically summarized as

$$\hat{L} = \arg \max_{L \in \mathcal{R}_L(\tilde{K})} \frac{\sum_{q=0}^{L_{f/2}} |\tilde{X}_{q\tilde{K}}(L)|^2}{L_r + L}, \quad (12)$$

$$\tilde{X}_{q\tilde{K}}(L) = \sum_{n=0}^{L_r-1} \tilde{x}(nT_b) \exp(-j2\pi q\tilde{K} \frac{n}{L_r + L}), \quad (13)$$

$$\mathcal{R}_L(\tilde{K}) = \{L_o, L_o + 1, \dots, L_o + 2L_\Delta\}, \quad (14)$$

$$\hat{\Delta} = \frac{(L_r + \hat{L})T_b}{\tilde{K}T_f} - 1, \quad (15)$$

The following remarks are in order.

Remark 1 A different length of the observation window is actually achieved in the discrete domain via padding a different number of zeros. This implies that \tilde{T}_o can only be increased or decreased with discrete steps of size T_b . The estimate of Δ is discrete. However, note that according to (15), the resolution of Δ is determined by both T_b and $\tilde{K}T_f$. The resolution of Δ can be improved by decreasing T_b or increasing $\tilde{K}T_f$. The sampling period T_b is restricted by the system hardware. The side-effect of increasing T_f will be addressed in the next remark. On the other hand, we have all freedom to increase \tilde{K} . It seems that if we can increase \tilde{K} infinitely, we can attain a Δ estimate with a super resolution. However, there are two factors to influence the main-lobe shape: the spectrum aliasing and the frame number of the transmitted signal N . We address the first one here, and discuss the second one in the next remark. Spectrum aliasing may shift the local peaks of the main lobes. Hence, even if we can infinitely increase \tilde{K} , we may not improve the resolution of Δ . Therefore, we need a well-designed front-end filter in order to avoid spectrum aliasing. On the other hand, increasing \tilde{K} will enlarge the search range of L and thus inflict a higher complexity in solving (12).

Remark 2 Note that the second factor changes the main-lobe shape through the side lobes from the other sinc pulses. Hence, it is desired that the main lobes are separated far enough to ignore the side-lobe effect, which can be achieved by increasing N to a reasonable number. Furthermore, if the main lobe of $\tilde{X}(f)$ is narrower, it is more robust against noise, which can be achieved by increasing N or T_f . Note that a larger T_f also helps to improve the resolution of Δ . But a larger NT_f takes a longer time for transmission. Hence, we choose T_f to be just long enough to avoid IFI. In summary, if we can carefully design the front-end filter to suppress the spectrum aliasing and choose a reasonable N to avoid the side-lobe effects, the proposed method can reach super resolution.

Remark 3 The proposed method does not need the knowledge of the multipath channel. Furthermore, the frequency domain analysis of the ranging signal is very useful. As it can be used to adopt super-resolution methods to estimate the TOA in the frequency domain, after we calibrate the clock skew.

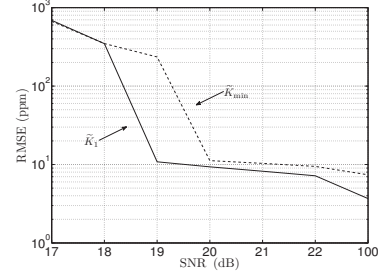


Fig. 4. RMSE of $\hat{\Delta}$

5. SIMULATION RESULTS

The performance of the clock skew estimation is evaluated by simulations using the IEEE 802.15.4a channel model CM1 - indoor residential LOS [7]. The frame period T_f is 200 ns to avoid IFI. The sampling period T_b is 0.5 ns. To speed up the simulation, we use $\Delta_{\max} = 2500$ ppm. Then, the Δ is randomly selected among $\{-2500$ ppm, -2450 ppm, \dots , 2500 ppm $\}$ in each run. The frame number of the ranging signal N is 100, and $N_\tau = 3$. Thus, we test $\tilde{K}_{\min} = 105$ and $\tilde{K}_1 = 195$. Moreover, $p(t)$ and $g(t)$ are the same as used in Fig. 4. The signal-to-noise ratio (SNR) is defined as the received signal strength to the noise ratio. Fig. 4 shows the RMSE of Δ vs. SNR. According to (15), we actually test discrete Δ s in the range of $\{-2500$ ppm, -2476.19 ppm, \dots , 2500 ppm $\}$ equally spaced with 23.81 ppm for \tilde{K}_{\min} , and in the range of $\{-2500$ ppm, -2487.18 ppm, \dots , 2500 ppm $\}$ equally spaced with 12.82 ppm for \tilde{K}_1 , respectively. Fig. 4 testifies that a larger \tilde{K} achieves a much better accuracy. In the noiseless case, the RMSE of \tilde{K}_1 is just half of the RMSE of \tilde{K}_{\min} .

6. REFERENCES

- [1] IEEE Working Group 802.15.4, "Part 15.4: Wireless Medium Access Control (MAC) and Physical Layer (PHY) Specifications for Low-Rate Wireless Personal Area Networks (LR-WPANs)," Dec. 2006.
- [2] S. Gezici, Z. Tian, G.B. Giannakis, H. Kobayashi, A.F. Molisch, H.V. Poor, and Z. Sahinoglu, "Localization via ultra-wideband radios: a look at positioning aspects for future sensor networks," *IEEE Signal Process. Mag.*, vol. 22, pp. 70–84, Jul. 2005.
- [3] S. Khalehosseini and J. Nielsen, "Cramer-Rao lower bound for data-aided and non-data-aided synchronisation of ultra-wideband signals with clock offset," *IET Commun.*, vol. 3, no. 1, pp. 135–142, Jan. 2009.
- [4] A. Wellig and Y. Qiu, "Trellis-based maximum-likelihood crystal drift estimator for ranging applications in UWB-LDR," in *Proc. IEEE Int. Conf. Ultra-wideband*, Sept. 2006, pp. 539–544.
- [5] Y. Wang, G. Leus, and H. Delic, "TOA estimation using UWB with low sampling rate and clock drift calibration," in *Proc. IEEE ICUWB*, Vancouver, Canada, Sept. 2009, pp. 612–617.
- [6] Xinrong Li and K. Pahlavan, "Super-resolution TOA estimation with diversity for indoor geolocation," *IEEE Trans. Wireless Commun.*, vol. 3, no. 1, pp. 224–234, Jan. 2004.
- [7] A.F. Molisch, K. Balakrishnan, C.C. Chong, S. Emami, A. Fort, J. Karedal, J. Kunisch, H. Schantz, U. Schuster, and K. Siwiak, "IEEE 802.15.4a channel model-final report," Tech. Rep., 2005.